Seismic performance of a novel self-sustaining beam-column connection for precast concrete moment-resisting frames

Seismic performance of a novel self-sustaining beam-column connection for precast concrete moment-resisting frames

Jia-Jun Fan[a,b], Gang Wu[a,b,*], De-Cheng Feng[a,b], Yi-Hua Zeng[a,b], Yong Lu[c]

a. Key Laboratory of Concrete and Prestressed Concrete Structures of the Ministry of Education, School of Civil Engineering, Southeast University, Nanjing 210096, China.

b. Laboratory of Industrialized Structural and Bridge Engineering of Jiangsu Province, Southeast University, Nanjing 210096, China

c. Institute for Infrastructure and Environment, School of Engineering, The University of Edinburgh, Edinburgh EH9 3JL, United Kingdom.

Abstract

In this paper, a novel prefabricated reinforced concrete (PC) self-sustaining beam-column connection for moment-resisting frames was developed to achieve the targets of short erection time, high construction efficiency, low-cost and satisfactory seismic performance. The connection design eliminates the need of temporary supports for the PC beams and slabs during the assembly process in site, and reduces the amount of lateral supports for PC multi-storey columns and formwork for cast-in-place concrete. As the designed thickness of PC U-shells at the beam ends was about 1/3 of the beam width, there could be a marked effect on the achieved integrity of such connections, especially under seismic loading. To investigate the seismic performance of this PC connection, five large-scale PC self-sustaining beam-column connections specimens and one reference conventional RC connection were designed and tested under reverse cyclic loading. The test parameters included the length and area of the flexural reinforcing bars placed at the bottom of PC U-shells, and the anchorage measures (stirrups) inside the PC U-shell. The five precast specimens exhibited similar crack distributions and failure patterns due to the gap-opening between the PC beams and column surface, which was attributed to the reduced effective width and depth of beam cross-section. The test results showed that the use of longer flexural reinforcing bars had little influence on the load-carrying capacity, but contributed to the initial stiffness and energy dissipation capacity. The load-carrying capacity increased by 24% when the area of flexural reinforcing bars increased by 50% in the U-shell region. The incorporation of stirrups in the overlapping region of beam flexural reinforcing bars and longitudinal rebars improved their bond-slip behaviour in specimen PC-S. Compared with specimen PC-C, the energy dissipation capacity of specimen PC-S was improved by 16.5%. Finally, the failure pattern and load-carrying capacity of

*Corresponding author at: School of Civil Engineering, Southeast University, Nanjing 210096, China.

the PC specimens were analysed and discussed using a simplified mechanical model.

Keywords: precast concrete; beam-column connection; self-sustaining connection; large-scale experiment; seismic performance; mechanical model.

1. Introduction and background

Over the past few decades, the industrialization of new building technologies based on prefabricated reinforced concrete (PC) structures has become a strategic subject due to its advantages of less manual labour, improved standardization and quality control, reduced environmental impact, high construction efficiency and good economic performance [1]. However, the seismic performance and integrity of a PC structure are essentially governed by the properties of the connections between various prefabricated units [2-4]. In the prefabricated reinforced concrete (PC) moment-resisting frames, the beam-column connections play an even more critical role in determining the overall structural performance. The damage and collapse of PC buildings caused by the failure of PC beam-column connections have been reported in many experimental studies and field observations after earthquake [5, 6]. From the structural point of view, an ideal PC beam-column connection should have the ability to transfer complex forces, maintain the integrity and prevent the collapse of the structure when used in the medium- and high-seismic regions [7-9]. Additionally, the assembly construction of the beam-column connections in site is complex, and this further resulted in the current practice of using heavily-distributed reinforcing bars in a rather confined space around a connection. Therefore, improving the connection technologies is a key to ensuring satisfactory seismic performance and constructability of PC frames [10, 11].

Various types of PC beam-column connections have been proposed and their seismic performance evaluated in the literature. These beam-column connections can be divided into two different categories based on their structural behaviour in comparison with their traditional cast-in-place (CIP) counterparts, namely, emulative beam-column connections and ductile connections [12-14]. In most cases, the ductile connections were semi-rigid and their rotational stiffness was smaller compared with cast-in-place connections. The energy dissipation capacity of ductility connections has been deemed to require enhancement with energy dissipation devices when used in seismic zones [10, 15]. For example, Ozturan et al. [16] tested the seismic performance of four types of ductile beam-column connections. The test results showed that the modified bolted connections had the advantages of easy fabrication and a good seismic performance. For the dry beam-column connection proposed by Vidjeapriya and Jaya [17], the prefabricated reinforced concrete (RC) columns and beams were connected with the cleat angle with different amounts of stiffener. Lacerda et al. [18] experimentally investigated the performance of a semi-rigid beam-column connection, in which the PC beams were

supported on the corbel of PC columns with continuity rebars.

On the other hand, in PC emulative beam-column connections the structural integrity of the beam-column connections is obtained through connecting the longitudinal reinforcing bars (or steel strand) of beams on two opposite sides of a connection crossing the columns and the casting concrete at the beam ends and joints. Such connections typically exhibit rigid behaviour which could closely match that of their cast-in-place counterparts. Thus, the conventional design methodologies and standards developed for RC structures may be appropriate for the emulative PC structures with minimal modification [19-21]. The emulative beam-column connections have been well accepted and widely used around the world. Various emulative beam-column connection technologies have been proposed and their seismic performance compared with the RC connections in the literature, as briefly summarised in the following.

Park and Bull [22] tested the performance of large-scale exterior beam-column connections consisting of PC columns and composite beams with U-shaped shells. Kim et al. [23] presented an experimental study about the developed cruciform PC beam-column connection. In this beam-column method, a PC beam shell was also adopted, and straight reinforcing bars were used for easy construction. The seismic performance of the precast connections was demonstrated to be acceptable. Parastesh et al. [24] reported the test results of interior and exterior beam-column connections suitable for PC frames located in high seismic zones. The precast concrete beams were designed with a hollow U-shaped cross-section, and the longitudinal reinforcing bars were spliced at the beam bottom before casting concrete. No slippage between PC components and the cast-in-place concrete was observed in spite of the smooth surface of the U-shaped section. The PC connections were demonstrated to be comparable with monolithic specimens in the aspects of flexural strength, ductility and energy dissipation. Hyeong et al. [25] conducted a cyclic loading test on large-scale emulative beam-column connections based on the previous research. In their research, the yield stiffness of the PC connection decreased by 10% and energy dissipation decreased by 36%, compared with the RC connection, because the PC beam shells were not completely integrated with the cast-in-place concrete and bond-slip in reinforcing bars occurred there. It was suggested that the thickness of the PC beam shell and the seating length be decreased to increase the effective cross-sectional area of the beam core and the depth of the joint. Considering the weakness of the PC beam-column connections, Eom et al. [26] proposed a plastic hinge relocation approach, including two strengthening methods and one weakening method, to improve the earthquake resistance of the beam-column connections by. Some researchers proposed different methods to connect the reinforcement of the opposite beams and these technologies were proved effective. Guan et al. [27] proposed a novel precast concrete beam-column connection, in which the precast beam with a U-shaped hollow area was also used. Pre-tensioned strands were used as the beam bottom reinforcement and connected through the bulb anchors

at the beam ends. Moreover, the additional bars inside the U-shaped hollow area were deemed necessary to provide adequate structural connections. From the literatures and discussion above, the use of U-shells at the PC beam ends has been found to be beneficial for an easy assembly construction and achieving an adequate flexural strength. However, the PC U-shells decrease the effective depth and width of the beam cross-section, and hence could be prone to an adverse impact on the integrity of the connections due to the difficulty in ensuring satisfactory bonding behaviour between the PC concrete and cast-in-place concrete. Moreover, the detailed continuity and anchorage measures for the arrangement of the reinforcement at the beam ends also could result in a significant effect on the seismic behaviour of the PC connections.

In some types of PC emulative beam-column connections, the PC beams were cast without the U-shell, and the connection and anchorage of the beam longitudinal reinforcing bars were achieved by different alternative methods. Xue and Zhang [28] developed a hybrid beam-column connection consisting of composite concrete beams and cast-in-place columns. Both the exterior and interior connections were demonstrated to behave similarly to the monolithic connections. In the experimental study conducted by Alcocer et al. [29], the continuity of the beam bottom reinforcement was achieved through the overlapping of U-shaped prestressing strands at the joint in one connection specimen. In the other connection specimen, the continuity of the reinforcement was obtained by placing the 90-degree hooks at the joint, and these hooks were tied in place and enhance by hoops around. Ha et al. [30] also used the U-shaped strands in their research to obtain an effective stress transfer mechanism. According to the test results, the proposed connections with transverse reinforcements were sufficient to use in moderate seismic regions. Yuksel et al. [31] studied the seismic performance of two different types of exterior beam-column connections, namely an industrial type and a residential type. Both connections showed high energy dissipation up to a 2% structural drift ratio.

Summarising the above overview, although various technologies of PC beam-column connections have been developed, they are generally complex and require much in-situ work to avoid unacceptable construction errors. Moreover, stabilising temporary supports for the prefabricated components and formwork for in-situ concrete casting are usually required, crippling the advantages of PC structures [32].

In this study, the proposed self-sustaining beam-column connections are aimed to be applied in conjunction with multi-storey precast columns with corbels. The connections are composed of PC beams with U-shells at beam ends, additional straight flexural reinforcing bars and cast-in-place concrete. The proposed PC self-sustaining beam-column connections were different with the existing PC connections in the larger thickness of PC U-shell and the corbel with sufficient strength on the PC column. The PC columns and beams can play the role of the vertical temporary supports, so no additional supports are required for the PC beams and slabs during the assembly construction on site. However, the

thickness of the PC U-shell are made markedly larger, and this introduced potential issue concerning the seismic behaviour of the PC connections. In the experimental study, additional straight reinforcing bars were placed inside the U-shell at the beam ends, through the beam-column joint and extended into the opposite beam as a remedial measure of the increased shell thickness. The cracking pattern and failure mode, load-carrying capacity, stiffness and strength degradation, ductility, strain distribution of reinforcement and concrete, and energy dissipation capacity of the PC connections were investigated to assess their seismic performance and compared with the cast-in-place specimen.

2. Description of the developed PC self-sustaining beam-column connections

The details of the PC self-sustaining beam-column connections are depicted in Fig. 1(a), and a photo of an actual project with this connection is shown in Fig. 1(b). It can been seen that the PC multi-storey columns were connected with the foundation through grouted sleeves and fixed with lateral supports. The precast beams with U-shells were directly seated on the corbels of the multi-storey precast column. The corbels of the PC columns and PC U-shells at beam ends were designed to carry both the self-weight of the PC components and the construction load. Similarly, the precast prestressed hollow core slabs were also designed to be seated on the PC composite beams (Fig. 1(b)). Overall, no temporary supports were required for the precast beams and slabs during the assembly process, that's why the proposed PC connections named “PC self-sustaining beam-column connection”.

The PC beam-column connections were easy to be completed after the prefabricated components were installed. Straight flexural reinforcing bars were placed at the bottom of the U-shell through the beam-column joint and extended into the opposite beam, and then concrete was cast at the joints and beam cores. The usage of straight reinforcing bars was convenient for assembly construction in site and avoided the congestion of reinforcing bars at the connection zone. There were no complex operations necessary for connecting the beam longitudinal reinforcing bars with mechanical splices or welding. Furthermore, the PC U-shells were used as permanent formworks for conveniently pouring concrete in site. Similarly, the assembly construction of the panel-to-structure (beam) connections contained connecting reinforcing bars protruding from PC hollow core slabs and casting concrete. Compared with various types of existing PC connections, the PC frames with this type of self-sustaining beam-column connections are also advantageous in terms of reduced erection time and good economic performance. However, it is understandable that the seismic performance of this connection would be influenced by some important parameters, including the length and area of flexural bars placed inside the U-shell, as well as the anchorage measures of the flexural reinforcing bars.

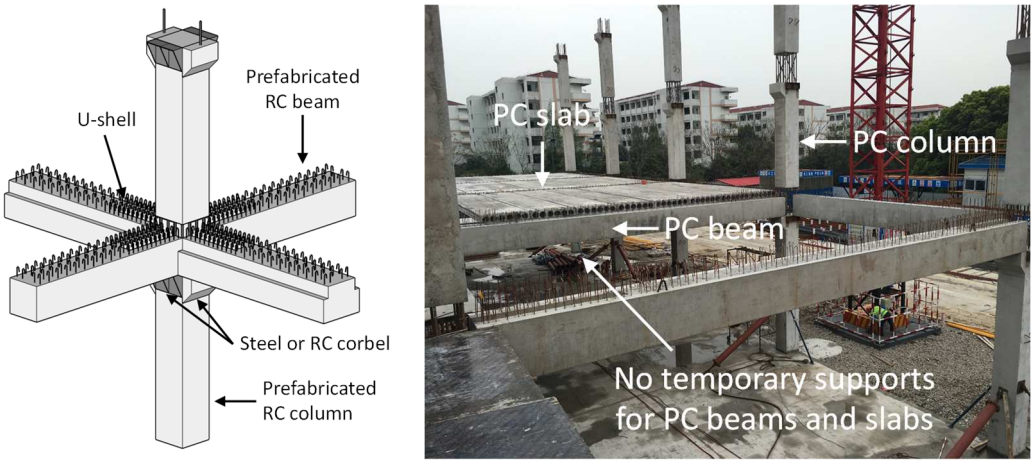

(a) Schematic (b) Photograph of an actual project

Fig. 1 The PC self-sustaining beam-column connections

3. Design and fabrication of test specimens

3.1 Description of test specimens

The five large-scale PC beam-column connections and the reference CIP specimen were re-designed based on the bottom storey of a pilot project in China (Fig. 1(b)). The prototype structure was a 4-storey building, in which the two levels at the bottom were used as an exhibition centre, and the two levels at the top were designed for office rooms. The storey heights of the first and second floors were 6 and 4.5 meters, respectively, and the dimensions of the column cross-section were 600 × 600 mm for both floors. The spans of the main beams were 8 and 12 meters in the longitudinal (along the length of the building) and transverse (along the width of the building) directions, respectively, to meet the requirement of large space. Considering a normal depth-span ratio of RC beams is 1/8-1/12 [33], the range of the beam depth was approximately 700-1000 mm. It should be mentioned that the precast prestressed hollow slabs (with a thickness of 200 mm) were placed upon the precast composite beams with the seating length of 75 mm. The side thickness of the PC U-shell was approximately 200 mm on average, therefore, the width of the precast beam was 600 mm, consistent with the width of the column.

The configurations, dimensions and reinforcement details of the test specimens are shown in Fig. 2. Each PC specimen was composed of one precast column without concrete at the joint, and two precast composite beams with U-shells. The cross-section was 600 × 600 mm for the PC columns and 600 × 800 mm for the composite beams after casting concrete. The PC beams were 3830 mm in length and the height of precast columns was 4650 mm, which were approximately the half lengths of the beams and columns in the prototype structure. The seating length of the PC beams on the PC column corbels was 180 mm (Fig. 2(a)). The longitudinal reinforcing bars of the PC columns were

10D28+2D25 mm, providing a reinforcement area of 7140 mm^2 and a reinforcement ratio of 1.98%. In the PC specimens, 6D25 and 2D16+4D10 rebars were placed at the bottom and top of the PC composite beams, respectively. However, all these bars were cut off at the beam ends and did not extend into the beam-column connections. The side thickness of the U-shell was 200 mm at top and 215 mm at bottom, and the bottom thickness was 70 mm (Fig. 2(b)). The inclined surface of the U-shell was designed to facilitate the removal of the formwork when the PC beams were fabricated. The flexural reinforcing bars were in straight without anchorage measures for convenient assembly construction. The lengths of the flexural reinforcing bars (4D20) inside the PC U-shell L_s were L_{ae}, $1.4L_{ae}$ and $1.6L_{ae}$ for specimens PC-L1, PC-C and PC-L2, respectively, with $L_{ae}=38D$ according to Chinese code [34], where L_{ae} is the anchorage length of tensioned reinforcing bars in concrete when components are under earthquake, and D is the diameter of the flexural reinforcing bars. In specimen PC-S (Fig. 2(c)), the flexural reinforcing bars and the rebars at the PC beam bottoms were colligated together with small U-stirrups. The small U-stirrups were 2D6 with a spacing of 100 mm. In specimen PC-R (Fig. 2(d)), 6D20 reinforcing bars were placed inside the U-shell, meaning that the reinforcement ratio of flexural reinforcing bars inside the U-shell was increased by 50%. In specimen CIP (Fig. 2(e)), 2D25 + 1D18 rebars were used as the longitudinal reinforcing bars at the bottom of RC beams, representing almost the same reinforcement area with the PC specimens. The depth of RC beams was 900 mm, considering the contribution of cast-in-place slabs. The test parameters and properties of the six specimens are summarized in Table 1. It should be mentioned that the influence of panel-to-structure connections was not considered in this research, and they might not adequate to allow for large seismic displacement demands and affected the overall system performance of the PC structures. [35, 36].

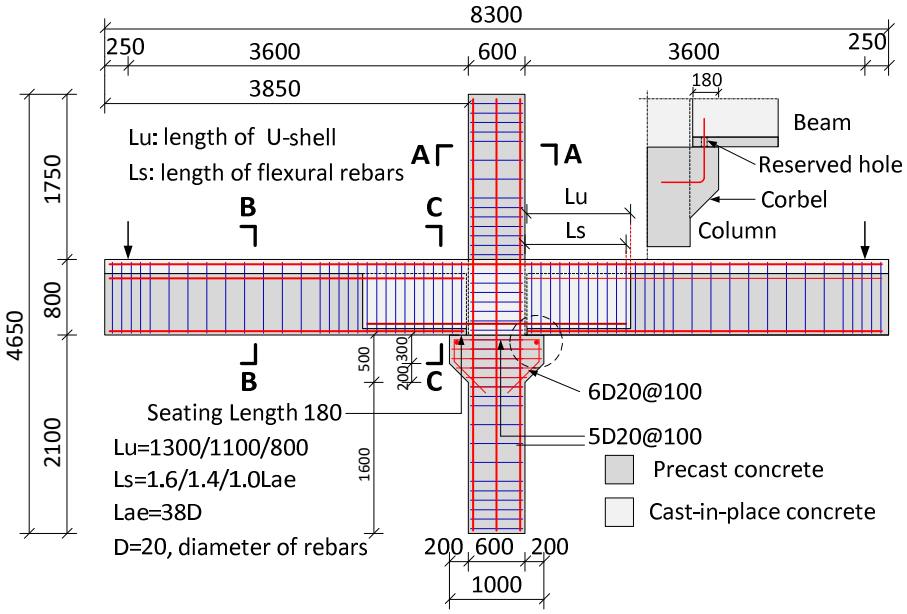

(a) Geometry of five PC specimens

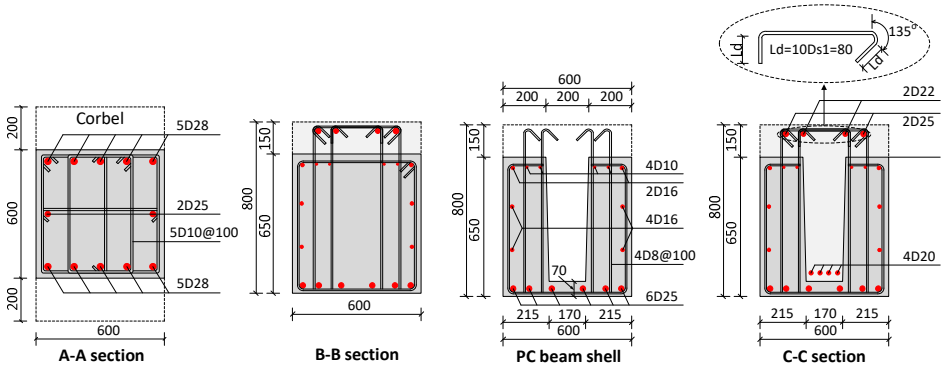

(b) Specimen PC-C, PC-L1 and PC-L2

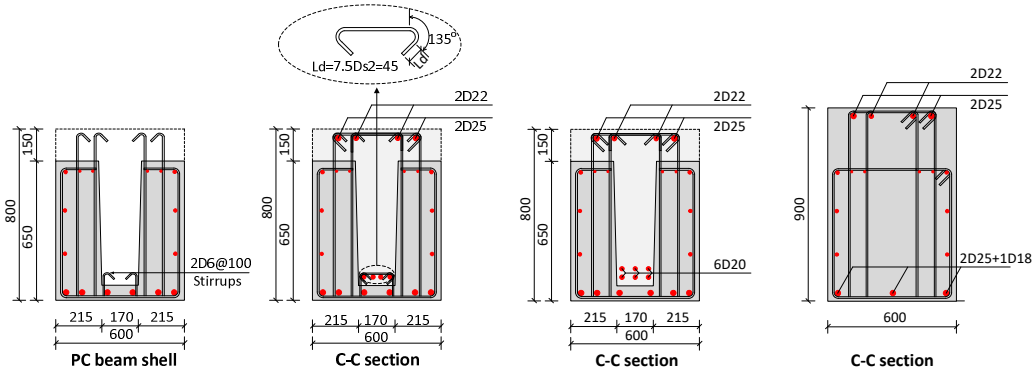

(c) Specimen PC-S (d) Specimen PC-R (e) Specimen CIP

Fig. 2. Configurations and reinforcement details of the test specimens (Dimensions in mm).

Table 1. Test parameters and properties of the test specimens

Specimen	Test parameter	L_s (mm)	L_u (mm)	Flexural rebars area
PC-C	Control specimen	$1.4L_{ae}$, 1065 mm	1100 mm	4D20, 1257 mm^2
PC-L1	Decreased flexural rebars length	L_{ae}, 760 mm	800 mm	4D20, 1257 mm^2
PC-L2	Increased flexural rebars length	$1.6L_{ae}$, 1220 mm	1300 mm	4D20, 1257 mm^2
PC-S	Stirrups inside U-shell	$1.4L_{ae}$, 1065 mm	1100 mm	4D20, 1257 mm^2
PC-R	Increased flexural rebars area	$1.4L_{ae}$, 1065 mm	1100 mm	6D20, 1885 mm^2
CIP	RC	--	--	2D25+1D18, 1491 mm^2

Notes: L_s is the length of flexural reinforcing bars inside the U-shell; L_u is the length of the PC U-shell at the beam ends.

The flexural rebars in specimen CIP were the longitudinal reinforcing bars at the bottom of the beam crossing the joint.

3.2 Assembly construction of PC connections

The specimen CIP and prefabricated components were made in a prefabrication factory and then transported to the

laboratory after the concrete strength met the requirement. Special attention was paid to the size and location of the U-shell at beam ends when the templates were made and the concrete was cast (Fig. 3). The assembly of five PC specimens were carried out in the laboratory. The main steps and key technical points during the assembly process are summarized as follows.

Step 1: all the surfaces of the precast concrete that made contact with the cast-in-place concrete were roughened and cleaned, including the surface inside the PC U-shell, the top surfaces of composite beams, and the top and bottom surfaces of the joint (Fig. 4(a) and (b)). This measure was beneficial for the adhesion strength between the precast concrete and cast-in-place concrete, ensuring the integrity of the connections and the composite beams after casting concrete. The roughness of the precast concrete surface was quantified by a parameter named the peak-to-valley height R_z, which represents the average of the maximum valley-to-peak-deviations within a certain number of assessment lengths [37]. In this experimental research, the R_z was more than 6 mm and classified as very rough.

Step 2: the precast column was lifted vertically and fixed on strong ground with lateral temporary supports. Then, the precast beams were lifted and installed upon the corbels of the PC column (Fig. 4(c)). The distance between the beam ends and the column surface was 20 mm. Vertical temporary supports were used under the precast beams, and these supports had enough strength and stiffness to resist the sum of the component weight and construction load. The locations of the precast beams and columns were checked with a laser horizontal instrument before the next step.

Step 3: the flexural reinforcing bars were placed at the bottom of the U-shell, crossing the joint and extending into the PC U-shell of the opposite beam. Meanwhile, the longitudinal reinforcing bars and stirrups were placed at the top of the PC composite beams. Finally, non-shrinkage fine aggregate concrete was cast in the beam-column joint and the top of composite beams. The two consecutive PC beams located at two sides of the PC column were connected with the joint consisted of the flexural reinforcing bars and cast-in-place concrete.

(a) U-shell (b) PC beam

Fig. 3. Prefabricated RC beams with a U-shell

(a) PC columns (b) PC beams (c) Assembly construction

Fig. 4. Fabrication of the PC beam-column connection

3.3 Properties of concrete and reinforcement

Ready-mixed C40 grade concrete was used for the CIP specimen and the prefabricated components of the five PC specimens. The concrete had a 28-day specified cube compressive strength (f_{cu}) of 40 MPa. The cast-in-place concrete used in PC specimens was ready-mixed non-shrinkage fine aggregate concrete with a higher compressive strength (that was C45 grade), having high flow characteristics. For both types of concrete, six 150 mm concrete cubes were moulded and cured in the same environment as the specimens. The concrete strength was tested under compression at 28 days and at the time when the connections were tested, respectively. For the C40 grade concrete, the average cube compressive strength at 28-days and at the time when the specimens were tested were 39.6 MPa and 43.5 MPa, respectively. For the C45 grade concrete, the average cube compressive strength at 28 days and at the time the specimens were tested were 46.2 MPa and 50.8 MPa, respectively. According to Chinese code GB50010 [33], the concrete axial compressive strength f_u was evaluated on the relationships as follow: $f_c = 0.88\alpha_{c1}\alpha_{c2}f_{cu}$, where α_{c1} is the ratio between axial compression and standard cube compression, for both the C40 and C45 grade concrete, and $\alpha_{c1}=0.76$. α_{c2} is the brittleness reduction factor of high strength concrete. For the C40 grade concrete, $\alpha_{c2}=1.0$; for the C45 grade concrete, $\alpha_{c2}=0.98$.

Hot rolled steel bars (HRB500) with a specified yield strength of 500 MPa were used for the longitudinal reinforcing bars in the beams and columns, also for the flexural reinforcing bars inside the U-shell. Hot rolled steel bars (HRB400) with the specified yield strength of 400 MPa were used as stirrups. Tension tests of the samples representing all types of rebars were conducted. The mechanical properties of the reinforcing bars are summarized in Table 2.

Table 2. Properties of the reinforcing bars

Diameter (mm)	D28	D25	D22	D20	D18	D16	D10	D8	D6
Types	HRB500						HRB400		
Area (mm^2)	616	491	380	314	254	201	79	50	28
Yield strength (MPa)	548	552	549	556	551	552	487	474	446

Ultimate strength (MPa)	714	721	728	741	727	725	614	631	602
Elastic modulus (GPa)	205	208	202	202	204	205	201	196	198

4. Test setup and loading procedure

The test setup and boundary conditions of test specimens are illustrated in Fig. 5 and Fig. 6. The adopted geometry of the tested specimens was determined by the spans of the beams and columns in the prototype structures, the loading space, as well as the stroke of the actuator and the distance between the ground anchors in the laboratory.

To simulate the roller boundary condition, both beam ends were attached to strong ground with long double-hinged links, also called roller supports. The double-hinged links at the beam ends allow horizontal translation and free rotation (zero moment), but restrict the vertical translation. The column bottom was attached to a hinge to achieve zero-moment, which can be regarded as the contra-flexural points of columns. The hinge was anchored on the strong floor with six D65 prestressed screws and restricted the horizontal movement during the loading process. Sixteen D15.2 prestressed steel strands (specified yield strength of 1860 MPa) were divided into four tendons to apply a constant vertical load of 3000 kN at the top of the column. The axial compressive ratio μ was approximately 0.43, which meets the requirement of Chinese Code, and is consistent with the prototype structure and common for multi-storey buildings [28, 33]. The axial compressive ratio μ is defined as $\mu = N/(A \bullet f_c)$, in which N is the applied axial load, A is the area of the column cross-section, and f_c is the axial compressive strength of the concrete. One hydraulic actuator with a 500 mm maximum stroke and ± 1000 kN loading capacity was used to apply the reverse cyclic loading at the top of the column. The clear span of the beam L_b, which is the length from the roller support to the column surface, was 3600 mm. The distance L between two roller supports at two beam ends was 7800 mm. The net length of the column H_c was 4675 mm, which is measured from the centre of the hinge at the column bottom to the lateral loading point (Fig. 5).

Three LVDTs (linear variable differential transformers) were placed at the bottoms of the supports under the column and beam ends to monitor any lateral movement of the support during the test. LVDTs were also installed at the top and bottom surfaces of the beam to measure the relative rotation between the column and beams. Reinforcement strain gages (gauge length 2 mm) and concrete strain gages (gauge length 100 mm) were used to measure the strain of the rebars and concrete at the beam ends and joints.

As shown in Fig. 7, a trail lateral drift ratio of 0.05% (approximately 2 mm) and a lateral load of 20 kN were applied once to check the operating condition of the test setup, loading system and the data acquisition before the formal cyclic loading. Based on the recommendations of ACI374.2-R13 [38] and FEMA-461 [39], the lateral loading protocol was

controlled by the lateral displacement [25, 26, 30]. Before a 1% lateral drift ratio, the applied lateral drift ratio was increased by a 0.25% increment. The increment was then increased to 0.5% in the loading process beyond 1% drift. Each displacement level was performed with three cycles to ensure stable crack propagation of the specimens. At each loading (displacement) step of each loading cycle, the hydraulic actuator was paused to observe the development of cracks, record the data of the applied displacement and load, and check the applied vertical load upon the column. The vertical compressive force was continually monitored and adjusted by the jacks and load cells attached to the four tendons of steel strands, so it was at the specified level with negligible variation during the test. The test was terminated when the applied load reduced to 85% of the ultimate lateral load, at which point the specimen was considered to have failed.

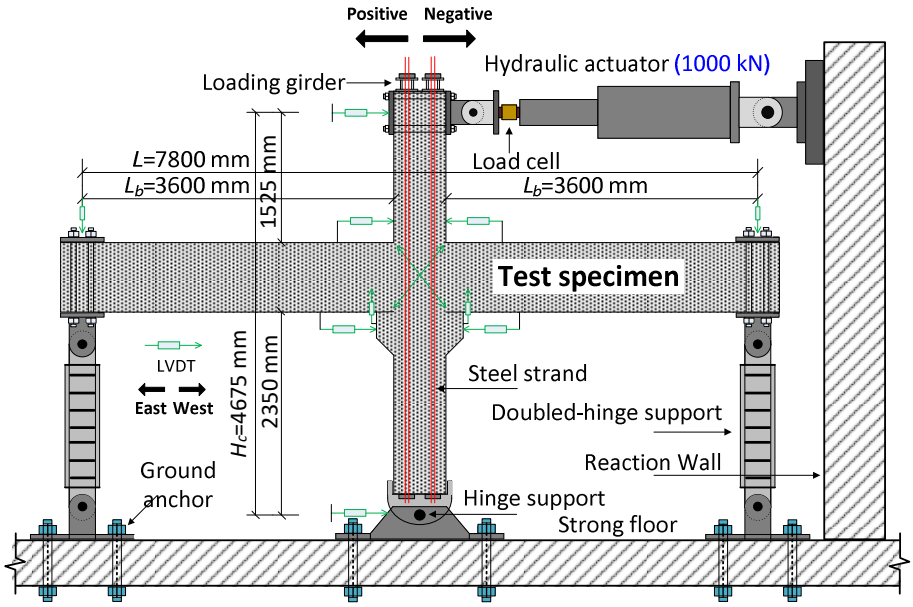

Fig. 5. Schematic of the test setup

Fig. 6. Photograph of the test setup

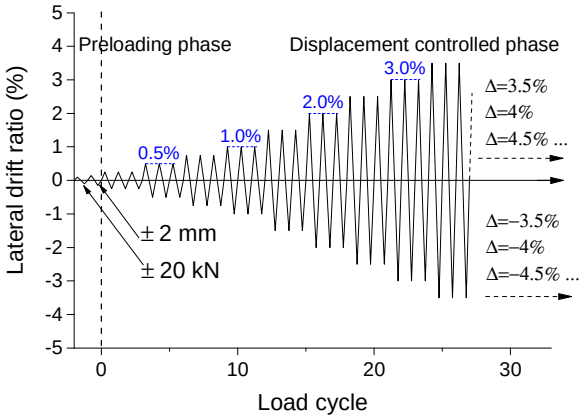

Fig. 7. Cyclic loading procedure

5. General behaviour of test specimens

5.1 Crack distributions and failure patterns

The concrete crack distributions and failure patterns of the six specimens are shown in Fig. 8. The five PC specimens exhibited similar crack progression during the loading process and failure patterns at the end of test, which were distinctly different from the CIP connection.

The failures of the five PC specimens were mainly attributed to the gap-opening between PC beams and the column surface, and a combination of the concrete crushing, rebar yielding and bond-slip at the beam ends and joints (Fig. 8(a) to (e)). For all the five PC specimens, a vertical crack between the precast beam end and column surface across the whole section was observed after a 0.5% lateral drift ratio. That was caused by the poor adhesion strength between the PC concrete and cast-in-place concrete despite the rough surface of PC concrete and higher strength of cast-in-place concrete [37]. Before the 1.5% lateral drift ratio, the gap between the PC beams and column surface opened and closed repeatedly under the reverse cyclic loading, resulting in concrete crushing. The range of the gap width was approximately 15-30 mm for the different PC specimens when the specimens failed. The gaps occurred at the beam ends was mainly attributed to the reduced effective depth and width of the beam cross-section due to the precast U-shell, as well as the large plastic strain of the reinforcing bars and the excessive bond-slip between the concrete and reinforcing bars. Compared with other existing PC beam-column connections, the decreased effective depth and width of the composite beam cross-section resulted in their different failure patterns, and no obvious plastic hinges occurred at beam ends in the five PC specimens. Vertical cracks and the spalling of the concrete cover occurred in the corbel under the large compression force after the 2% lateral drift ratio in the PC specimens, except specimen PC-R where no significant damage occurred in the corbel. In specimen CIP, the failure was attributed to the severe diagonal shear cracking and bond-slip of the beam longitudinal reinforcing bars at the joint (Fig. 8(f)). The serious joint damage was attributed to the large depth of the beam, which was 1.5 times of the column width and resulted in the “strong-beam and weak column”.

Specimen PC-S is taken as an example to show the development of cracks under increased reverse cyclic loading and the failure pattern (Fig. 8(d)). During the three cycles of the 0.25% lateral drift ratio, the vertical cracks between the PC beams and column surface developed quickly and nearly crossed the whole section. Meanwhile, two vertical flexural cracks appeared at the top of the beam at the distances of 350 mm and 600 mm from the column surface. The flexural cracks were with the lengths of approximately 150 mm, just equal to the thickness of the cast-in-place concrete. At the first cycle of the 0.5% lateral drift ratio, several distributed flexural cracks occurred along the beams at both the top and bottom within the distance of 1400 mm from the column surface, with a spacing of about 250-350 mm. When the lateral

drift ratio reached 0.75%, the gaps between the precast beam and corbel were observed, indicating the PC beams rotated along the column. An across-section vertical flexural crack was observed at a distance of 1100 mm from the column surface, just at the end of the PC U-shell. At the lateral drift ratio of 1%, the gaps at both beam ends became obvious, with the largest width of 3.5 mm, and closed after unloading. Meanwhile, several diagonal shear cracks were observed at the joint. The width of the gaps at beam ends increased to approximately 8 mm at the third cycle of the 1.5% lateral drift ratio. When the lateral drift ratio reached 2%, a horizontal crack with a length of approximately 180 mm was observed at the top of the cast-in-place joint. It should be noted that the horizontal crack there did not cross the whole section of the column until the end of test. At the first cycle of the 2.5% lateral drift ratio, the diagonal shear cracks at the joint developed quickly, and vertical cracks were observed on the column corbels. At the lateral drift ratio of 3%, the width of the gap between the PC beam and column surface was approximately 22 mm, with many small cracks around the gap. Meanwhile, pieces of concrete were dropped from the gap, indicating the concrete was crushed under compression inside the beam.

A sound indicating a bar fracture was noticed at the top of the PC beams at the third cycle of the 3.5% lateral drift ratio, companied with the sudden drop of the applied load (Fig. 9(d)). The specimen PC-S failed because of a low-cycle fatigue fracture of the reinforcing bars at top of the beam [40]. This failure pattern was explained as follows. After the 2% lateral drift ratio, buckling of the reinforcing bars at the top of the beam occurred due to the increased compression strength, crushing of concrete and local damage of the stirrups there. Under the reverse cyclic loading, the reinforcing bars suffered repeated bending and tension deformation and finally fractured at the end of test. It was observed that the corbel under the PC beams to some extent restricted the rotation along the column downwards, reducing the deformation ability of the beam-column connection.

In spite of the similar development of cracks, there was still some difference in the failure patterns of the five PC specimens. In specimens PC-L2 and PC-R, the obvious horizontal cracks were observed at the top of composite beams, which was caused by the poor adhesion strength between the PC concrete and cast-in-place concrete. The diagonal shear cracks in the PC-R specimen were more serious than the other four PC specimens; however, the damage of the corbel in the PC-R specimen was minor. The width of the gap at the beam ends in the PC-L1 specimen was approximately 30 mm on average when the specimen failed, which is larger than that of the other four specimens. Additionally, the corbel damage, diagonal shear cracks at the joint and concrete crushing at beam ends in the specimen PC-L1 were more serious compared with the specimens PC-C and PC-L2.

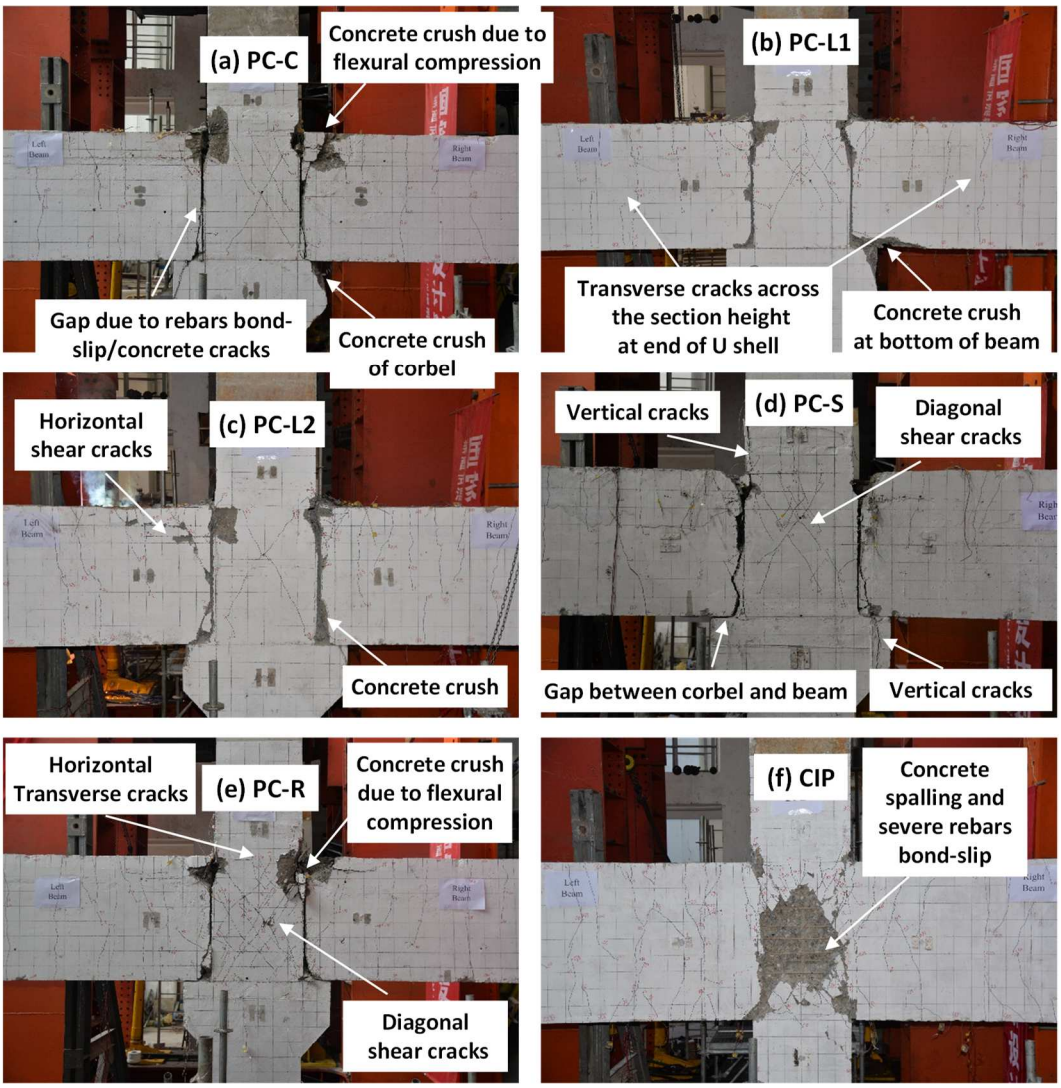

Fig. 8. Crack distributions and failure patterns of the test specimens

5.2 Lateral load-drift ratio relationships

The lateral load-displacement (drift ratio) relationships of the six tested specimens are shown in Fig. 9(a) to (f). The envelop curves of the hysteresis loops are plotted in Fig. 9(g). The lateral drift ratio was calculated by dividing the lateral displacement by the effective height of the column (H_c = 4675 mm, Fig. 5). In this research, the yielding strength was not obvious and involved higher uncertainty due to the displacement controlled loading procedure. The yield lateral drift ratio Δ_y and ultimate lateral drift ratio Δ_u were defined by using the equivalent elasto-plastic energy principle proposed by Park [41]. As shown in Fig. 9(h), when the area A_1 is equal to the area A_2, the position of point H can be determined. Then, the yield point Y was obtained by the intersection of line HG (parallel to the vertical axis) and the envelop curves. The ultimate lateral drift ratio Δ_u was defined as the post-peak lateral drift ratio when the load dropped to 85% of the maximum strength P_{max}.

The yield lateral ratio Δ_y, yield strength P_y, maximum strength P_{max}, corresponding drift ratio Δ_m, ultimate drift ratio Δ_u, and ductility μ of the test specimens in both the positive and negative directions are summarized in Table 3.

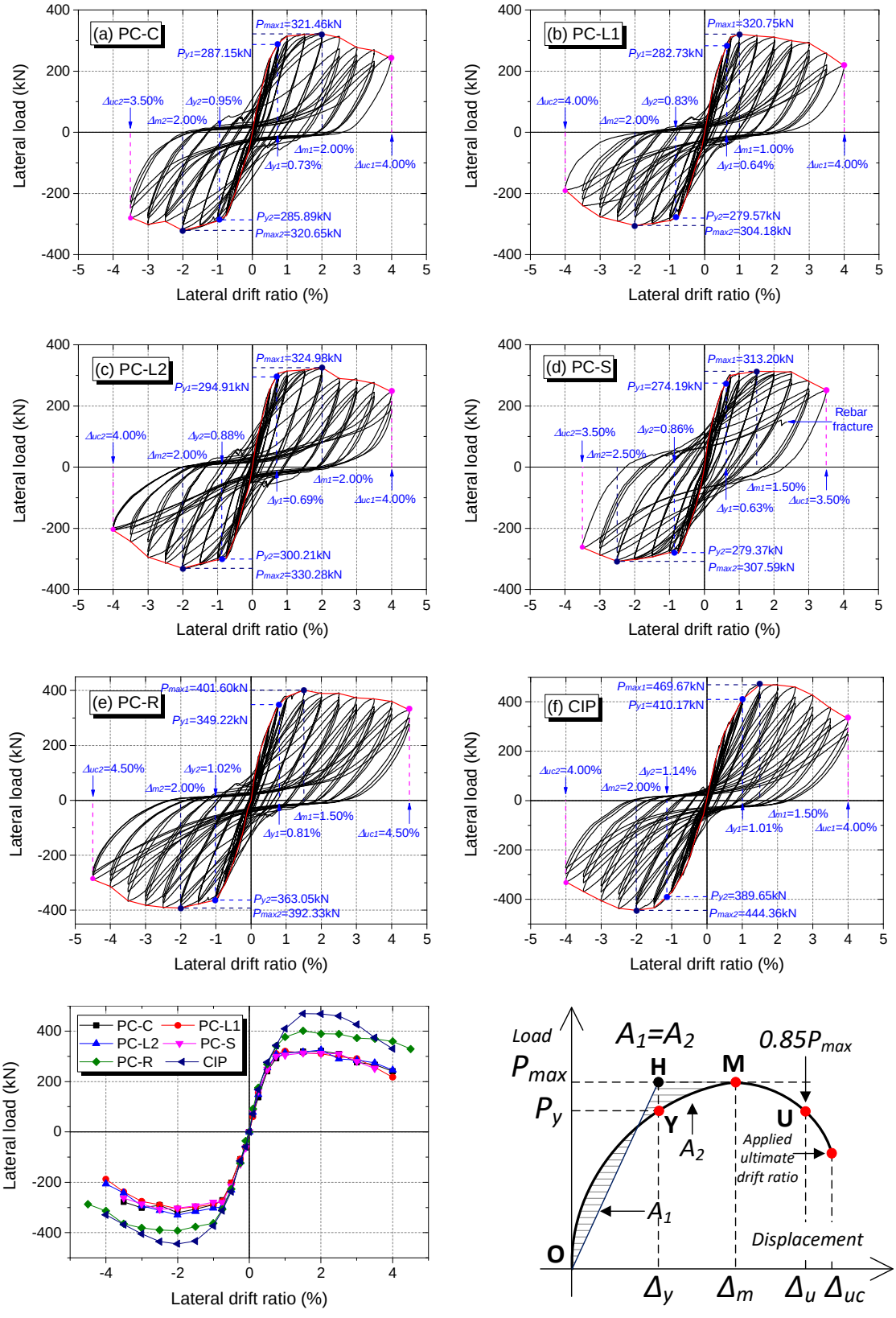

(g) Envelops curves (h) Equivalent elasto-plastic energy principle

Fig. 9. Lateral load-drift ratio relationships of the test specimens

Notes: Δ_{uc} in Fig. 9(a) to (f) represented the ultimate lateral drift ratio of the applied loading cycle, and the corresponding load was less than 85% of the normal maximum load.

In Fig. 9(a) to (c), the specimens PC-C, PC-L1 and PC-L2 showed similar overall cyclic behaviour despite of their different lengths of the U-shells and flexural reinforcing bars. Yielding of the specimens PC-C, PC-L1 and PC-L2 occurred at the 0.64%-0.95% lateral drift ratio in the positive direction and negative directions. After the peak load, the load-carrying capacities of the specimens PC-C, PC-L1 and PC-L2 decreased gradually and failed at the lateral drift ratio of 3.01%-3.37%. Taking the negative direction for example, the yield strength of specimen PC-L2 was 300.2 kN at a lateral drift ratio of 0.88%, while the yield strength of specimen PC-L1 was 279.6 kN at a lateral drift ratio of 0.83%. The yield strength of specimen PC-L2 was larger than the PC-L1 specimen, which was attributed to the decreased bond-slip between the flexural reinforcing bars and the cast-in-place concrete due to the longer anchorage length. However, the PC-C, PC-L1 and PC-L2 specimens exhibited little difference in the peak strength, which was attributed to the failure patterns described in Fig. 8(a) to (c).

The hysteretic loops of specimen PC-S (Fig. 9(d)) were less pinching compared with the control specimen PC-C, indicating that more energy was dissipated. This finding revealed that the stirrups inside the U-shell enhanced the anchorage performance of the flexural reinforcing bars and increased the yielding length of the flexural reinforcing bars at the beam ends and joint. After yielding, the load-carrying capacity of specimen PC-S was maintained. The maximum strength of specimen PC-R was 401.6 kN and 392.3 kN in the positive and negative directions, respectively (Fig. 9(e)), showing an improvement by approximately 24% on average as compared with specimen PC-C. Moreover, the yielding lateral drift ratio Δ_y and the ultimate lateral drift ratio Δ_u also improved. The CIP specimen had a higher load-carrying capacity compared with the five PC specimens (Fig. 5 (f)); however, the hysteretic loop showed more pinching. After the maximum strength, the strength of the CIP specimen decreased quickly, exhibiting poor ductility. The poor energy dissipation capacity and ductility were attributed to the serious shear damage at the joint.

Table 3. Test results of the test specimens

Specimen	**Load direction**	Δ_y **(%)**	P_y **(kN)**	Δ_m **(%)**	P_{max} **(kN)**	Δ_u **(%)**	μ
PC-C	positive	0.73	287.2	2.00	321.5	3.20	4.39
	negative	0.95	285.9	2.00	320.7	3.01	3.17
PC-L1	positive	0.64	282.7	1.00	320.8	3.27	5.11

	negative	0.83	279.6	2.00	304.2	3.22	3.88
PC-L2	positive	0.69	294.6	2.00	325.0	3.37	4.88
	negative	0.88	300.2	2.00	330.3	3.13	3.56
PC-S	positive	0.63	274.2	1.50	313.3	3.01	4.78
	negative	0.86	279.4	2.50	307.6	2.99	3.48
PC-R	positive	0.81	349.2	1.50	401.6	4.02	4.96
	negative	1.02	363.1	2.00	392.3	3.81	3.74
CIP	positive	1.01	410.2	1.50	469.7	3.28	3.25
	negative	1.14	389.7	2.00	444.4	3.39	2.97

Notes: The ductility $\mu = \Delta_u/\Delta_y$ was calculated by the ratio of the ultimate lateral drift ratio Δ_u to the yielding lateral drift ratio Δ_y.

5.3 Strain of reinforcement and concrete

Because of the similar failure patterns of the five PC specimens, specimen PC-S is taken as an example to examine the strain distributions of the rebars and concrete. Fig. 10 shows the measured strain of the concrete and rebars during the loading process, including the longitudinal reinforcing bars at the top and bottom of the beams, the flexural reinforcing bars inside the U-shell, and the concrete at beam ends. The lateral displacement plotted in the x-axes in all the plots in Fig. 10 (b) and (c) was the applied lateral displacement at the loading point. In each plot, the vertical blue dotted line and number represented the applied lateral drift ratio.

SC1 represented the measured strain of the concrete at a distance of 750 mm from the column surface, and SC2 was at a distance of 700 mm from the column surface (Fig. 10(a) and (b)). The strain of SC1 was under tension during the application of both positive and negative load and reached more than 2000 με at a 2% lateral drift ratio in the positive direction. Combined with the vertical transfer cracks there, it was evident that the bond-slip of the longitudinal rebars in the beams occurred there. SC2 showed that the concrete in this area was under compression with the positive load and under tension with the negative load. The longitudinal reinforcing bars at the top of the beam at a distance of 400 mm from the column surface (SR2 in Fig. 10(c)) reached the yield strain (approximately 2500 με) at a 1.5% lateral drift ratio. Then, the strain of reinforcing bars there dropped quickly, which was caused by the bond-slip of the rebars, crushing of concrete, and rebar buckling at different loading stages. This finding was also confirmed by the increasing strain of the same rebars (SR1 in Fig. 10(c)), which remained at approximately 2000 με until the end of test.

SR3, SR4, SR5 (Fig. 10 (c)) represented the strain of the flexural reinforcing bars inside the PC U-shell at different locations. The flexural reinforcing bars at the beam ends, with a distance of 50 mm from the column surface (SR3 in Fig.

10(a)), developed large tensile strain under the reverse cyclic loading. The flexural reinforcing bars there yielded at the 0.75% lateral drift ratio with the strain of more than 2500 με, and then reached approximately 4500 με at the 1.5% lateral drift ratio. The development of the strain in the flexural reinforcing bars was accompanied with the concrete cracking and gap-opening at the beam ends. With the increasing of applied lateral drift ratio, the bar yielding penetrated into the joint. The flexural reinforcing bar at the joint, with a distance of 150 mm from the column surface (S4 in Fig. 10(a)), developed large plastic tension and compression strain under the reverse cyclic loading and yielded at the 2% lateral drift ratio. These results indicated that yielding and bond-slip of the flexural reinforcing bar occurred at the joint, which was also proved by the diagonal shear cracks (Fig. 8). The tension strain of the flexural reinforcing bar reached approximately 2000 με at the 2% lateral drift ratio at a distance of 500 mm from the column surface (S5 in Fig. 10(a)), and then declined rapidly due to rebar bond-slip and the concrete crushing at the bottom of the beam. It should be noted that the PC beam bottom longitudinal reinforcing bars (S6 in Fig. 10(a)), developed large compression strain of approximately 1300 με (remained elastic) at the 2% lateral drift ratio at the beam end. Then, the compression strain of the reinforcing bars decreased because of the concrete crushing and bond-slip.

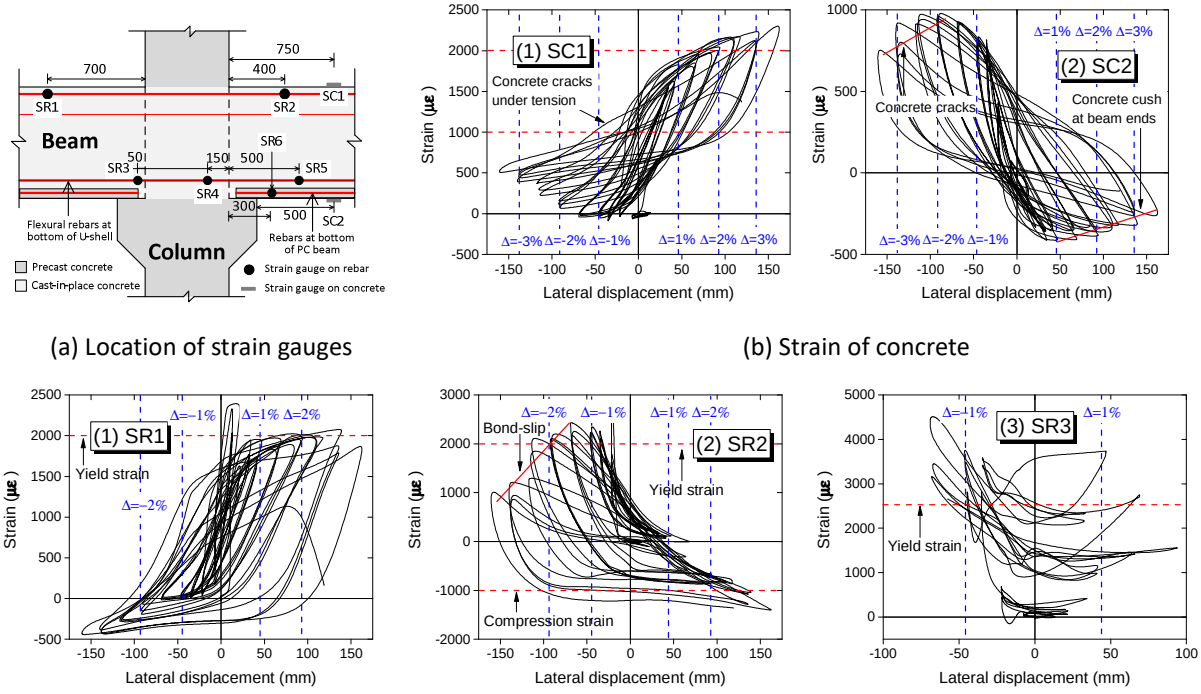

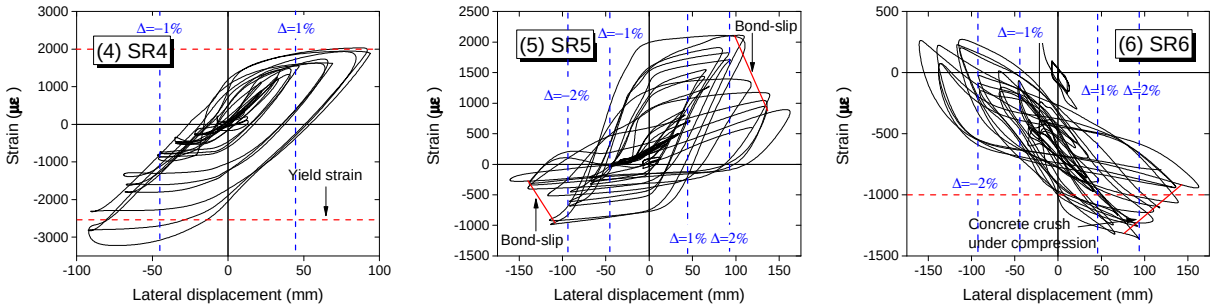

(c) Strain of reinforcing bars

Fig. 10. Measured strain of the concrete and rebars in specimen PC-S

5.4 Simplified mechanical model and load-carrying capacity

According to the crack distributions and failure patterns (refer to Fig. 8(a) to (e)), as well as the hysteretic loops and load-carrying capacity, the failures of all the five PC connections exhibited a beam yielding mechanism and the critical region was located at the beam ends. Therefore, the load-carrying capacity of the PC self-sustaining beam-column connections under considerations depended on the moment-carrying capacity of the critical beam cross-sections. On the basis of the test results discussed above, a simplified mechanical model for the precast connection involving a U-shell precast beam was established, as shown in Fig. 11, to calculate the load-carrying capacity. According to the schematic shown in the test setup (Fig. 5), the relationship between the applied load at the top of column P_n and the moment-carrying capacity at the critical regions (M_{bL} and M_{bR}) can be calculated as Eq. (1).

$$M_{bL} + M_{bR} = (P_{bL} + P_{bR}) \cdot L_b = \frac{2P_n H_c}{L} \cdot L_b \quad (1)$$

As shown in Fig. 11(a), without considering the contribution of corbels for the negative moment, $M_{bL}= P_{bL}\cdot L_b$, $M_{bR}= P_{bR}\cdot L_b$. M_{bL} and M_{bR} represented the moments at the left and right beam ends, respectively. P_{bL} and P_{bR} were the vertical reaction forces of the roller supports at the left and right beam ends, respectively. Before 1.5% lateral drift ratio, the moments M_{bL} and M_{bR} increased rapidly, resulting in the increasing of the applied lateral load P_n (shown in Fig. 9), causing the concrete cracking and flexural reinforcing bars yielding. After that, the moment M_{bL} and M_{bR} decreased due to the serious concrete crushing, bond-slip of flexural reinforcing bars and longitudinal rebars, and large gap at beam ends, as shown in Fig. 8.

Combined with the failure pattern, deformation, and strain distributions of concrete and reinforcing bars, a simplified beam yielding mechanical model for the moment-carrying capacity at the left and right beam ends can be established, as shown in Fig. 11(b) and (c). When calculating the positive moment M_{bL}, the thickness of the U-shell was taken as the effective depth and width of the beam. Additionally, the reinforcing bars (6D25) at the bottom of the PC beams had no

contribution to the moment capacity because these bars had no tension stress (refer to SR6 in Fig. 10(c)). However, in the calculation of the negative moment M_{bR}, the contribution of the reinforcing bars (6D25) at the beam bottom and the PC U-shell should be considered. It should be noted that the corbels also contributed to the negative moment capacity M_{bR} because the corbels restricted the relative rotation of the right beam along the column, changing the area and height of the compression zone at the bottom of the beam, also providing the vertical force at beam end. However, the corbels had no influence on the positive moment capacity M_{bL} because there was a small gap-opening observed between the PC beam and the corbel under positive moment (Fig. 8).

The simplified mechanical model was consistent with the crack distributions and failure patterns of the PC self-sustaining beam-column connections. When the specimen was under positive load, the tension reinforcing bars at the top of the right beam were anchored to the compression zone of the left beam because of the gap at the beam end and the bond-slip of the rebars in the joint region (refer to SR1 and SR2 in Fig. 10 (c)). Therefore, the compression zone at the left beam end was subjected to the combination of compression and anchorage forces (Fig. 11(b)). At that time, the reinforcing bars at the top of the right beam were anchored in the cast-in-place concrete, where distributed vertical cracks occurred. Under reverse cyclic loading, horizontal shear cracks were observed between the cast-in-place and PC concrete at the tops of the beams with the lengths of 200-550 mm for the different PC specimens. In specimen PC-R, there were more flexural reinforcing bars at the bottom of the U-shell, which meant a larger A_{s1} when calculated the positive moment M_{bL} at the critical region (Fig. 11(b)). Hence, the local damage and concrete crushing at the top of the beam at the critical region was more serious (Fig. 8(e)). Meanwhile, more diagonal shear cracks at the joint and longer horizontal shear cracks at the top of the PC composite beam were observed due to the increased shear force and severe bond-slip of the rebars at the joint.

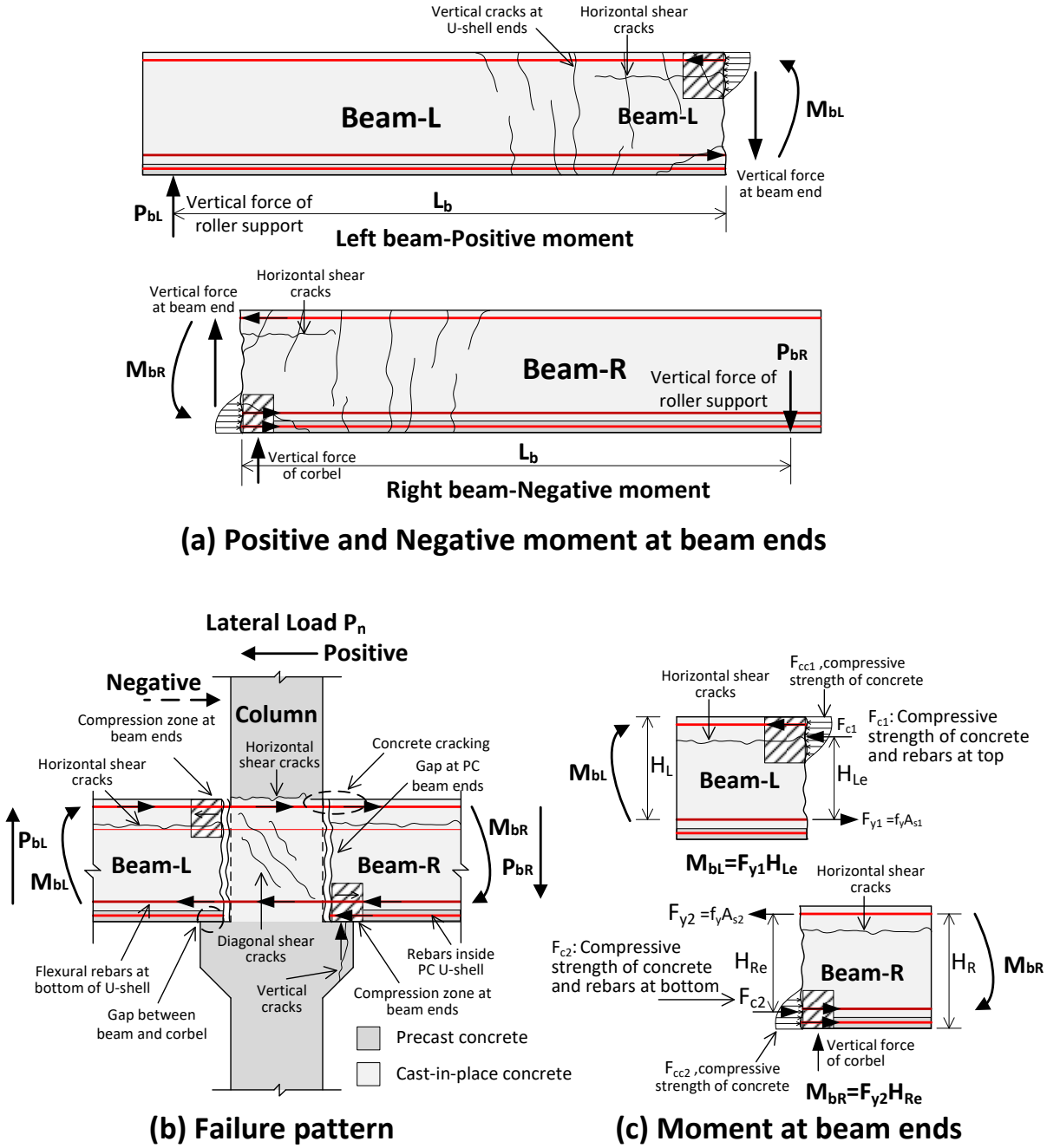

Fig. 11. Simplified mechanical model of the PC connection.

Take specimen PC-C for an example to verify the mechanical model. The actual material strength and rectangular concrete stress block of ACI 318-08 [42] were used in the calculation. For the different diameters of reinforcing bars (refer to Table 1), the ultimate tensile stress f_y = 720 MPa was used to simplify the calculation. In the calculation of the positive moment at the left beam ends, H_{Le}=610 mm was obtained from the equation: F_{y1}=F_{c1}. Hence, the positive moment can be calculated as M_{bL}= F_{y1}·H_{Le}=1257 mm^2×720 MPa×610 mm=560 kN·m. Due to the complex stress at the right beam ends, the contribution of the corbel to the negative moment M_{bR} was not considered to simplify the calculation. The

distance H_{Re} between the tension force of the rebars at the top of the beam and the centre of the compression force of the rebars and concrete was 550 mm. The negative moment at the right beam ends was calculated as $M_{bR}= F_{y2}\cdot H_{Re}$=1742 mm^2×720 MPa×550 mm= 689 kN·m. The theoretical load-carrying capacity of the PC-C specimen was calculated as $P_n = (M_{bL} + M_{bR})\cdot L/L_b/H_c/2$ =289 kN. The tested load of the PC-C specimen was 320 kN on average, which was 10.7% larger than the calculation. This was attributed to the exclusion of the contribution of the corbel for the negative moment-carrying capacity and the reinforcing bars at the top of the PC U-shell (2D16+4D10) for the positive moment-carrying capacity. For specimen PC-R, a similar conclusion was also obtained, which was about 12% less than the test results.

6. Cyclic performance indicators of test specimens

6.1 Stiffness and strength degradation

The magnitudes of the secant stiffness of the six specimens at each loading lateral drift ratio, i.e. the stiffness degradation [43], are compared in Fig. 12. The stiffness degradation essentially reflects the cumulative damage of a structural element under seismic load and is an important factor for the evaluation of the overall response. For the five PC specimens, the secant stiffness decreased continuously with the increasing applied displacement due to the cumulative damage during the loading process. Before the 1.5% lateral drift ratio, the scant stiffness decreased rapidly, which was attributed to the development of concrete cracking, bond-slip and yielding of the reinforcing bars. After that, the gap at the beams was not closed after unloading and the stiffness degradation dropped slowly. Specimen PC-R exhibited larger secant stiffness compared with the other four PC specimens, and is attributable to more reinforcing bars inside the U-shell. The length of the reinforcing bars inside the U-shell had little influence on the degradation. However, the PC-L2 specimen possessed the largest initial scant stiffness, followed by specimen PC-S, indicating that an adequate anchorage ability of the flexural reinforcing bars was beneficial to the initial stiffness.

The cumulative damage could also result in strength degradation during the three repeated cycles at a given lateral displacement level. The strength degradation can be defined as the ratio of the cyclic load-carrying capacity at the i^{th} (i=2,3) load cycle to that at the first load cycle, as shown in Fig. 13 and Eq. (2).

$$\alpha_i = \frac{P_j^i}{P_j^1} \tag{2}$$

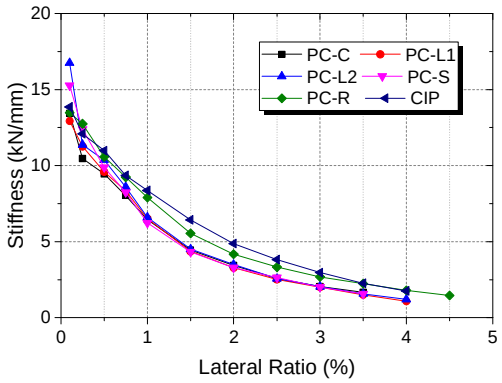

Fig. 12 Stiffness degradation

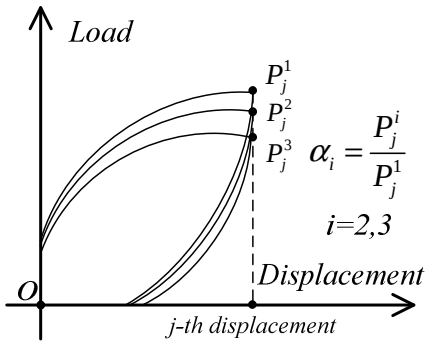

Fig. 13 Definition of the strength degradation ratio

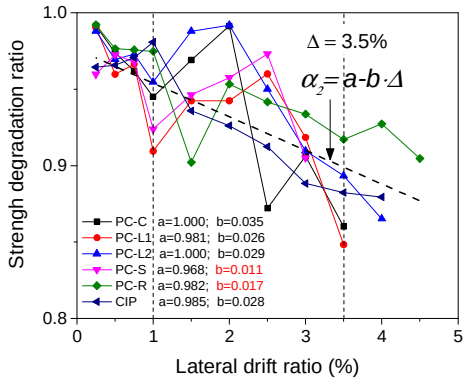

(a) Strength degradation ratio in the second cycle

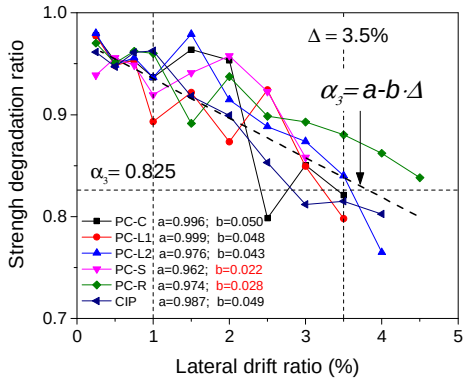

(b) Strength degradation ratio in the third cycle

Fig. 14. Strength degradation ratios of the test specimens

In the specimens PC-C, PC-L1, PC-L2 and PC-S, there was a sudden drop of the strength degradation ratios in both the second and third cycles (α_2 and α_3) at the 1% lateral drift ratio, then increased at the 1.5% and 2% lateral drift ratios (Fig. 14(a) and (b)). The sudden drop of the strength degradation ratio also occurred in specimen PC-R at the 1.5% lateral drift ratio. The sudden drop was attributed to the large gap-opening at the beam ends. Although the load-carrying capacity was similar, the strength degradation in specimen PC-L1 was more serious compared with the specimens PC-C and PC-L2, indicating that the shorter length of the flexural reinforcing bars increased the cumulative damages. In specimens PC-C, PC-L1, PC-L2, the strength degradation ratios α_2 and α_3 decreased by 3.0% and 4.8% on average, at every 1% lateral drift ratio, respectively. However, the PC-S and PC-R specimens showed different strength degradation ratios α_2 and α_3, which decreased by 1.4% and 2.5% on average, respectively. These results showed that more reinforcing bars and stirrups inside the PC U-shell were beneficial for mitigating strength degradation of the PC beam-column connections. In the five PC specimens, the strength degradation ratio α_3 at the 3.5% lateral drift ratio was approximately 0.825 on average, which was greater than 0.75 according to the acceptance criteria specified by ACI 374.1-05 [44]. For specimen CIP, the strength

degradation ratios α_2 and α_3 were basically linear due to the diagonal shear crack damage at the joint region.

6.2 Energy dissipation capacity

The energy dissipation capacity of test specimens is calculated and compared in terms of the energy dissipation per load cycle, energy dissipation per load level, cumulative energy dissipation and the equivalent viscous damping ratio, as shown in Fig. 15(a) to (d). The energy dissipation per load cycle is defined as the area enclosed by a load-displacement cycle, and the energy dissipation per load level is defined as the sum of the three load-displacement cycles at a given displacement. The cumulative energy dissipation is evaluated as the total energy dissipation up to a given draft ratio level. The definition of the equivalent viscous damping ratio ζ_{eq} is shown in Fig. 15(e) [45]. Where $S_{(ABC+CDA)}$ denotes the area enclosed by the hysteresis loop at a given displacement, $S_{(\Delta OBE+\Delta ODF)}$ denotes the sum of the area of the two right triangles OBE and ODF.

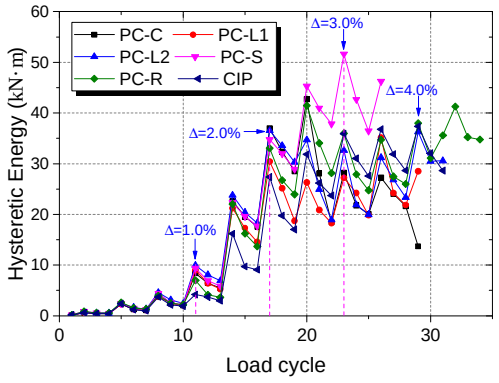

(a) Energy dissipation per load cycle

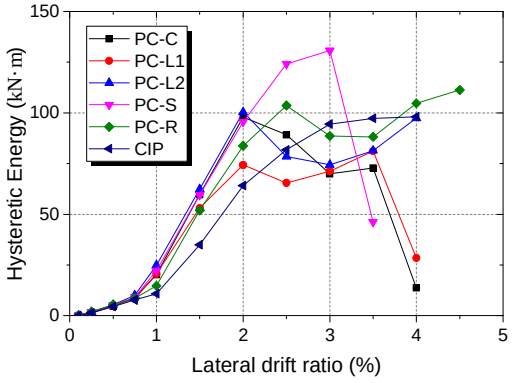

(b) Energy dissipation per load level

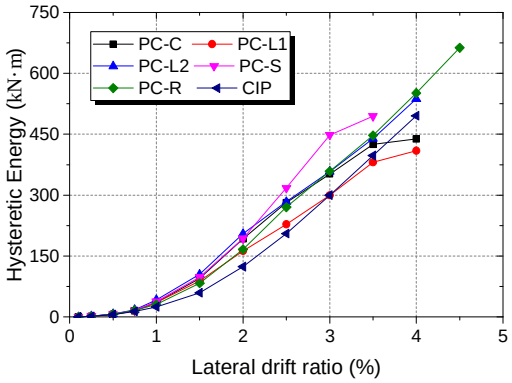

(c) Cumulative energy dissipation

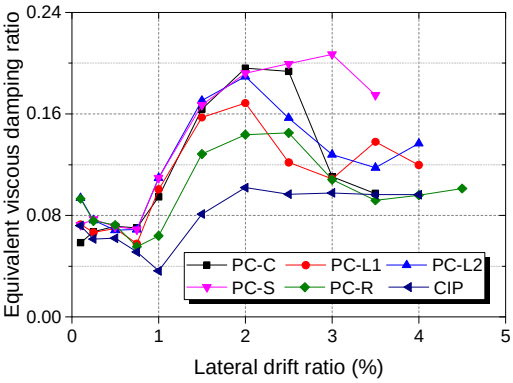

(d) Equivalent viscous damping ratio

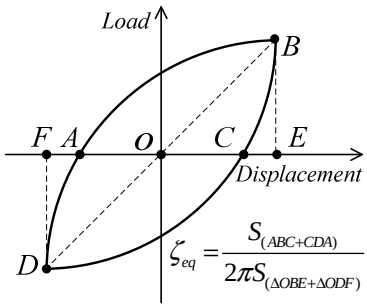

(e) Definition of the equivalent viscous damping ratio

Fig. 15. Energy dissipation capacity of the test specimens.

In specimen PC-C, the energy dissipation per load cycle reached a maximum value at the first cycle of the 2.5% lateral drift ratio, while the maximum value in specimen PC-S was achieved at the first cycle of the 3% lateral drift ratio. The equivalent viscous damping ratio and energy dissipation per load level in specimen PC-S continued to increase until a lateral drift ratio of 3% and were much larger than those of the PC-C specimen. Finally, the cumulative energy dissipation of specimen PC-S was 16.5% greater than that of specimen PC-C. Hence, in spite of their similar load-carrying capacities, the usage of stirrups inside the PC U-shell reduced the bond-slip of the flexural reinforcing bars and increased the energy dissipation capacity, demonstrating the efficiency and advantages of this anchorage measure.

Among the three specimens PC-L1, PC-C and PC-L2, the PC-L1 specimen exhibited the lowest amount of energy dissipation and an equivalent viscous damping ratio. The cumulative energy dissipation of specimen PC-L1 was 31.1% less than that of specimen PC-L2 at the 4% lateral drift ratio, indicating a better energy dissipation capacity of the PC beam-column connection with longer flexural reinforcing bars inside the PC U-shell. In spite of the higher load-carrying capacity and larger ultimate lateral drift ratio, the differences of energy dissipation capacity between specimens PC-R and PC-C were minor at the same lateral drift ratio before 3.5%. This finding was attributed to the significant rebar bond-slip and more damage at the joint in specimen PC-R, resulting in more pronounced pinching of the hysteretic loops and smaller equivalent viscous damping ratios (Fig. 15(d)). Due to non-ideal damage at the joint in specimen CIP, the equivalent viscous damping ratio was smaller compared to those of the PC specimens, and the energy dissipation capacity was unsatisfactory considering its higher load-carrying capacity.

7. Conclusions

Precast concrete frames with self-sustaining beam-column connections have been proposed and implemented in several pilot buildings in China. The proposed PC connections have great advantages in terms of high construction

efficiency, less manual labour, cost effectiveness, and less need for formworks and temporary supports, as have been demonstrated by the test specimens in the laboratory and actual projects. Large-scale experiments were performed to study the seismic performance of the PC self-sustaining beam-column connections. On the basis of the test results, the following conclusions can be drawn:

(1) The PC self-sustaining beam-column connections showed a distinctly different failure pattern compared with normal cast-in-place connections. Such a failure pattern was characterised by a gap-opening between the PC beams and column, combined with concrete crushing, rebar yielding and bond-slip at the beam ends and joints. The large gap-opening was attributed to the PC U-shell with large thickness at the beam ends, resulting in a decreased effective depth and width of the PC beam cross-section.

(2) The corbels of the PC columns are key to enable easy assembly and a short overall erection time of this type of PC frames in site. At the same time, the corbels also contribute to the load-carrying capacity, including the negative moment-resisting capacity and shear resistance at the beam ends. However, the corbels restricted the relative rotation of the beams to columns, especially in negative bending, and this effect has been shown to result in a decreased deformation capacity and earlier fracture of the top longitudinal reinforcing bars at the beam top.

(3) The straight flexural reinforcing bars inside the PC U-shell resulted in the different failure pattern compared with the existing similar PC connections. The length of the flexural reinforcing bars inside the PC U-shell had little influence on the load-carrying capacity of the PC connections. Nevertheless, the longer flexural reinforcing bars in specimen PC-L2 increased the energy dissipation capacity because of the reduced rebar bond-slip at the beam ends, and also improved the initial stiffness.

(4) Compared with specimen PC-C, the load-carrying capacity of specimen PC-R improved by 24% when the area of the flexural reinforcing bars was increased by 50%. In addition, the ultimate lateral drift ratio also improved by 22% on average. The more flexural reinforcing bars inside the PC U-shell tended to have contributed to the stiffness and strength degradation.

(5) In specimen PC-S, anchorage measures (stirrups) used to colligate the flexural reinforcing bars inside the U-shell and the PC beam bottom longitudinal rebars together were demonstrated to be effective in enhancing the energy dissipation capacity, as well as mitigating the strength degradation.

(6) The simplified mechanical model with the beam yielding mechanism was consistent with the crack distributions, failure pattern, strains of the reinforcing bars and concrete. In the five specimens, the theoretical load-carrying capacities based on the simplified mechanical models were consistent with the test results but slightly underestimate by

approximately 9.5%-14%. This underestimation was due to the exclusion of the constructional reinforcement at the top of PC composite beams and the contribution of corbels to simplify the calculation.

The test results suggest that from the seismic performance point of view, the side thickness of the precast U-shell at the beam ends should be smaller to ensure the load-carrying capacity and improve the integrity of the PC connections. On the other hand, sufficient side thickness of the PC U-shell is required for the assembly construction in site. Hence, there is a scope for optimization of the designed PC U-shell in terms of the length, thickness, inside surface and stirrups in order to achieve both good constructability and satisfactory seismic performance. Furthermore, economic performance between the PC connections and CIP connections should be compared and analyzed in the future.

The details of the self-sustaining beam-column connections in PC frames are on course to be adopted in the Chinese code for the design of precast concrete structures. Further study should look into possible measures for enhancing the integrity between the U-shell PC beam and the cast-in-place joint, thus avoiding large gap-opening at the beam ends. Extended experimental studies are also recommended to cover a wider range of parameter variation for precast concrete frames with self-sustaining beam-column connections to fully estimate the seismic behaviour of the building and increase the application in moderate- and high-seismic regions.

Acknowledgements

The authors acknowledge financial support from the National Key Research and Development Program of China (No. 2016YFC0701400), the National Natural Science Foundation of China (Grant Nos. 51838004, 51525801), the Natural Science Foundation of Jiangsu Province (Grant No. BK20170680).

References

[1] Kurama YC, Sritharan S, Fleischman RB, Restrepo JI, Henry RS, Cleland NM, et al. Seismic-Resistant Precast Concrete Structures: State of the Art. Journal of Structural Engineering 2018; 144(4): 03118001.

[2] Loo Y, Yao B. Static and repeated load tests on precast concrete beam-to-column connections. PCI journal 1995; 40(2): 106-115.

[3] Restrepo JI, Park R, Buchanan AH. Tests on connections of earthquake resisting precast reinforced concrete perimeter frames of buildings. PCI journal 1995; 40(4): 44-61.

[4] Biondini F, Toniolo G. Probabilistic calibration and experimental validation of the seismic design criteria for one-storey concrete frames. Journal of Earthquake Engineering 2009; 13(4): 426-462.

[5] Brunesi E, Nascimbene R, Bolognini D, Bellotti D. Experimental investigation of the cyclic response of reinforced precast concrete framed structures. PCI Journal 2015; 60(2): 57-79.

[6] Belleri A, Brunesi E, Nascimbene R, Pagani M, Riva P. Seismic performance of precast industrial facilities following major earthquakes in the Italian territory. Journal of Performance of Constructed Facilities 2015; 29(5): 04014135.

[7] Feng D, Xie S, Ning C, Liang S. Investigation of Modeling Strategies for Progressive Collapse Analysis of RC Frame Structures. Journal of Performance of Constructed Facilities 2019; 33(6): 04019063.

[8] Choi H, Choi Y, Choi C. Development and testing of precast concrete beam-to-column connections. Engineering Structures 2013; 56: 1820-1835.

[9] Precast/Prestressed Concrete Institute. PCI - Design handbook: precast and prestressed concrete, 7th ed. Chicago, IL; 2010.

[10] Huang Y, Mazzarolo E, Briseghella B, Zordan T, Chen A. Experimental and numerical investigation of the cyclic behaviour of an innovative prefabricated beam-to-column joint. Engineering Structures 2017; 150: 373-389.

[11] Feng D, Xie S, Deng W, Ding Z. Probabilistic failure analysis of reinforced concrete beam-column sub-assemblage under column removal scenario. Engineering Failure Analysis 2019; 100: 381-392.

[12] Bahrami S, Madhkhan M, Shirmohammadi F, Nazemi N. Behavior of two new moment resisting precast beam to column connections subjected to lateral loading. Engineering Structures 2017; 132: 808-821.

[13] ACI Committee 550. Guide to emulating cast-in-place detailing for seismic design of precast concrete structures (550.1R-09). Farmington Hills (MI): ACI; 2009.

[14] Breccolotti M, Gentile S, Tommasini M, Materazzi A, Bonfigli M, et al. Beam-column joints in continuous RC frames: Comparison between cast-in-situ and precast solutions. Engineering Structures 2016; 127: 129-144.

[15] Alva G, de Cresce El. Moment-rotation relationship of RC beam-column connections: Experimental tests and analytical model. Engineering Structures 2013; 56: 1427-1438.

[16] Ozturan T, Ozden S, Ertas O. Ductile connections in precast concrete moment resisting frames. concrete construction, 2006; 9: 11.

[17] Vidjeapriya R, Jaya K. Experimental study on two simple mechanical precast beam-column connections under reverse cyclic loading. Journal of Performance of Constructed Facilities 2012; 27(4): 402-414.

[18] Lacerda M, da Silva T, Alva G, de Lima M. Influence of the vertical grouting in the interface between corbel and beam in beam-to-column connections of precast concrete structures–An experimental analysis. Engineering Structures 2018; 172: 201-213.

633 [19] Popa V, Papurcu A, Cotofana D, Pascu, R. Experimental testing on emulative connections for precast columns using
634 grouted corrugated steel sleeves. Bulletin of Earthquake Engineering 2015; 13(8): 2429-2447.
635 [20] Feng D, Wu G, Lu Y. Finite element modelling approach for precast reinforced concrete beam-to-column connections
636 under cyclic loading. Engineering Structures 2018; 174: 49-66.
637 [21] Kataoka M, Ferreira M, de Cresce El. Nonlinear FE analysis of slab-beam-column connection in precast concrete
638 structures. Engineering Structures 2017; 143: 306-315.
639 [22] Bull D, Park R. Seismic resistance of frames incorporating precast prestressed concrete beam shells. PCI journal
640 1986; 31(4): 54-93.
641 [23] Kim S, Moon J, Lee L. An experimental study of the structural behavior on the precast concrete beam-column interior
642 joint with splice type reinforcing bars. J. Archit. Inst. Korea 2004; 20(10): 53-61.
643 [24] Parastesh H, Hajirasouliha I, Ramezani R. A new ductile moment-resisting connection for precast concrete frames
644 in seismic regions: an experimental investigation. Engineering Structures 2014; 70: 144-157.
645 [25] Im H, Park H, Eom T. Cyclic Loading Test for Reinforced-Concrete-Emulated Beam-Column Connection of Precast
646 Concrete Moment Frame. ACI Structural Journal 2013; 110(1): 115-126.
647 [26] Eom T, Park H, Hwang H, Kang S. Plastic Hinge Relocation Methods for Emulative PC Beam–Column Connections.
648 Journal of Structural Engineering 2015; 142(2): 04015111.
649 [27] Guan D, Guo Z, Xiao Q, Zheng Y. Experimental study of a new beam-to-column connection for precast concrete
650 frames under reversal cyclic loading. Advances in Structural Engineering 2016; 19(3): 529-545.
651 [28] Xue W, Zhang B. Seismic behavior of hybrid concrete beam-column connections with composite beams and cast-in-
652 place columns. ACI Structural Journal 2014; 111(3): 617-627.
653 [29] Alcocer S, Carranza R, Perez-Navarrete D, Martinez R. Seismic tests of beam-to-column connections in a precast
654 concrete frame. PCI journal 2002; 47(3): 70-89.
655 [30] Ha S, Kim S, Lee M, Moon J. Performance evaluation of semi precast concrete beam-column connections with U-
656 shaped strands. Advances in Structural Engineering 2014; 17(11): 1585-1600.
657 [31] Yuksel E, Karadogan H, Bal İE, Ilki A, Bal A, Inci P. Seismic behavior of two exterior beam–column connections
658 made of normal-strength concrete developed for precast construction. Engineering structures 2015; 99: 157-172.
659 [32] Feng D, Ren X. Enriched Force-Based Frame Element with Evolutionary Plastic Hinge. Journal of Structural
660 Engineering 2017; 143(10): 06017005.
661 [33] Chinese Code, Code for Seismic Design of Buildings (GB50011-2010), Chinese Building Press, Beijing, China,

662 2010. (in Chinese)
663 [34] Chinese Code, Code for Design of Concrete Structures (GB50010-2010), Chinese Building Press, Beijing,
664 China, 2010. (in Chinese)
665 [35] Bournas D, Negro P, Molina FJ. Pseudodynamic tests on a full-scale 3-storey precast concrete building: Behavior of
666 the mechanical connections and floor diaphragms. Engineering Structures 2013; 57: 609–627.
667 [36] Brunesi E, Bolognini D, Nascimbene R. Evaluation of the shear capacity of precast-prestressed hollow core slabs:
668 numerical and experimental comparisons. Materials and Structures 2015; 48(5): 1503-1521.
669 [37] fib International Federation for Structural Concrete. Model code 2010. Lausanne: fib; 2010.
670 [38] ACI Committee 374. Guide for testing reinforced concrete structural elements under slowly applied simulated
671 seismic loads (374.2 R-13). Farmington Hills (MI): ACI; 2013.
672 [39] Federal Emergency Management Agency (FEMA). Interim Testing Protocols for Determining the Seismic
673 Performance Characteristics of Structural and Nonstructural Components, Report No. FEMA-461, 2007.
674 [40] Higai T, Nakamura H, Saito S. Fatigue failure criterion for deformed bars subjected to large deformation
675 reversals. Special Publication 2006; 237: 37-54.
676 [41] Park R. Evaluation of ductility of structures and structural assemblages from laboratory testing. Bulletin of the
677 New Zealand national society for earthquake engineering 1989; 22(3): 155-166.
678 [42] ACI Committee 318. Building code requirements for structural concrete (ACI 318-08) and commentary.
679 Farmington Hills (MI): ACI; 2008.
680 [43] Sucuoglu H. Effect of connection rigidity on seismic response of precast concrete frames. PCI journal 1995;
681 40(1): 94-103.
682 [44] ACI Committee 374. Acceptance criteria for moment frames based on structural testing and commentary (ACI 374.1-
683 05). Farmington Hills (MI): ACI; 2005.
684 [45] Chopra AK. Dynamics of structures: theory and applications to earthquake engineering. Prentice-Hall, 2001.